check for updates

ARTICLE

Topology Optimization for Harmonic Excitation Structures with Minimum Length Scale Control Using the Discrete Variable Method

Hongliang Liu[1], Peijin Wang[1], Yuan Liang[2,*], Kai Long[3] and Dixiong Yang[2]

[1]Key Laboratory of Liaoning Province for Composite Structural Analysis of Aerocraft and Simulation, College of Aerospace Engineering, Shenyang Aerospace University, Shenyang, 110136, China

[2]State Key Laboratory of Structural Analysis for Industrial Equipment, Department of Engineering Mechanics, Dalian University of Technology, Dalian, 116023, China

[3]State Key Laboratory for Alternate Electrical Power System with Renewable Energy Sources, North China Electric Power University, Beijing, 102206, China

*Corresponding Author: Yuan Liang. Email: yuanliangdut@dlut.edu.cn

ABSTRACT

Continuum topology optimization considering the vibration response is of great value in the engineering structure design. The aim of this study is to address the topological design optimization of harmonic excitation structures with minimum length scale control to facilitate structural manufacturing. A structural topology design based on discrete variables is proposed to avoid localized vibration modes, gray regions and fuzzy boundaries in harmonic excitation topology optimization. The topological design model and sensitivity formulation are derived. The requirement of minimum size control is transformed into a geometric constraint using the discrete variables. Consequently, thin bars, small holes, and sharp corners, which are not conducive to the manufacturing process, can be eliminated from the design results. The present optimization design can efficiently achieve a 0–1 topology configuration with a significantly improved resonance frequency in a wide range of excitation frequencies. Additionally, the optimal solution for harmonic excitation topology optimization is not necessarily symmetric when the load and support are symmetric, which is a distinct difference from the static optimization design. Hence, one-half of the design domain cannot be selected according to the load and support symmetry. Numerical examples are presented to demonstrate the effectiveness of the discrete variable design for excitation frequency topology optimization, and to improve the design manufacturability.

KEYWORDS

Discrete variable topology optimization; harmonic excitation; minimum length scale control; geometric constraint; manufacturability

1 Introduction

Topology optimization can result in innovative structural designs via the determination of the optimal material distribution under predefined constraints without prior knowledge. In recent years, structural topology optimization has been developed rapidly and applied extensively. Various optimization methods have become effective tools for engineering structure design [1,2], such as

homogenization-based method [3], density-based SIMP (solid isotropic material with penalization) method [4–6], evolutionary optimization method [7], independent continuous mapping method [8], level-set method [9,10], component-based optimization method [11], and feature-driven optimization method [12]. These approaches have been extensively used to solve various structural design problems.

Because engineering structures require an increasing level of dynamic performance, topology optimization involving structural vibration characteristics is critical [13–16]. Currently, topology optimization considering structural dynamic performance is garnering attention. The study includes topology optimization under harmonic excitation [17–23], topological optimization with fundamental frequency maximization [24–29], topological optimization considering high-order natural frequency maximization or frequency bandwidth optimization [30,31], and the corresponding indicators for measuring the structural vibration effect as constraints for modeling [32,33]. Zargham et al. [34] provided a comprehensive review of structural dynamic topology optimization based on different optimization methods.

Structural topology optimization that considers external harmonic excitation has received considerable attention. Ma et al. [35] performed a study to minimize structural dynamic compliance under volume constraints. When the excitation frequency exceeded the first resonance frequency, the structural dynamic compliance minimization with volume constraints was investigated [36]. In this case, invalid locally optimal solutions may be yielded, and static compliance constraints can be added to avoid such a phenomenon. Meanwhile, Niu et al. [19] compared different objective functions, and stress-constrained topology designs were achieved [37]. Notably, the density-based method is the most widely applied method to topology design under harmonic excitation. However, the optimization results contain unavoidable gray areas (intermediate densities), particularly when considering the inertial effect of harmonic excitation. Intermediate densities may cause numerical problems in dynamic topology optimization, i.e., typically localized vibration modes [38], which need to be addressed via additional techniques [39]. By merely truncating the intermediate densities, the objective function associated with the harmonic excitation may be degenerated significantly. Meanwhile, gray regions and fuzzy boundaries are not conducive to the extraction and control of geometric information from the optimization result; furthermore, they affect the structural manufacturing [40].

To improve manufacturability, topological design considering minimum length scale control is crucial. Furthermore, it is an efficient technique for addressing numerical instabilities in design optimization, such as mesh dependence and checkerboard patterns [41]. Although density filtering can avoid mesh dependence and checkerboard patterns, the gray region formed at the structural boundary expands as the filtering radius increases, which implies that the minimum length scale cannot be strictly controlled. Additionally, three-field SIMP methods utilizing nonlinear projection techniques tend to yield 0–1 designs, and the minimum size may not be strictly satisfied [42,43]. Based on the three-field SIMP method, a robust formulation considering corrosion and expansion operations as well as a geometric constraint method without additional finite element analysis were proposed [44,45]. Meanwhile, the minimum length scale control of the topology design can be imposed using a structural skeleton [46] and an image morphology operator [47]. It is worth noting that the length scale control was not applied to the topology optimization of harmonic excitation structures in previous studies. Many thin bars, small holes, and sharp corners may appear in the optimization results of harmonic excitation structures. Thus, clear and smooth topology designs with minimum length scale control are desirable for the manufacturing process.

Symmetry is an important and appealing property for structural topology optimization, as it significantly reduces the computational cost. The symmetry of optimal solutions in structural topology optimization has received significant attention [48–50]. However, when the loading and support

conditions are symmetric, the existence of the symmetric property in the harmonic excitation topology design problem should be verified.

In the present work, a topological design method based on discrete variables [51] is employed to resolve the topology optimization of harmonic excitation structures with length scale control. The discrete variable method is based on SAIP (sequential approximate integer programming) and CRA (canonical relaxation algorithm), which can avoid gray problems and achieve clear 0–1 solutions in topology optimization [52,53]. Compared with the branch-and-bound method [54], it exhibits polynomial time complexity; thus, its computational efficiency is higher. In addition, unlike the Lagrange relaxation method, it does not require the solving of non-smooth dual optimization problems [55]. Compared with the well-known evolutionary structure optimization method [56], it can manage multiple constraints via a unified mathematical programming framework, such as the size control constraints discussed herein. In this study, an optimization model is established by considering the structural dynamic compliance optimization under volume constraints, and the corresponding sensitivity formulas are derived. Furthermore, results show that the topology design solution of the harmonic excitation optimization problem may not necessarily be symmetric, even when the load and support are symmetric, which is different from the static compliance problem.

2 Discrete Variable Topology Optimization under Harmonic Excitation

2.1 Objective Function of Design Optimization

The motion equation of the harmonic excitation problem can be expressed as [19]

$$M\ddot{u} + C\dot{u} + Ku = Fe^{i\omega t} \tag{1}$$

where K and M denote stiffness and mass matrices, respectively; C denotes the damping matrix; $\ddot{u}$ and $\dot{u}$ represent acceleration and velocity, respectively; F is the prescribed amplitude; ω is the excitation frequency. By setting $u = Ue^{i\omega t}$, where U denotes the displacement amplitude, the governing equation can be rewritten as

$$\left(K - \omega^2 M + i\omega C\right) U = F \tag{2}$$

Subsequently, the following equation can be obtained

$$U^{\mathrm{T}} \left(K - \omega^2 M + i\omega C\right) U = U^{\mathrm{T}} F \tag{3}$$

The structural dynamic compliance is defined as

$$c = F^{\mathrm{T}} U \tag{4}$$

Here, $c = c_R + ic_S$, where c_R and c_S are the real and imaginary components of c, respectively. When the excitation frequency ω is zero, the dynamic compliance can be degenerated into static compliance.

In this study, the square of the dynamic compliance is employed as the objective function for topology optimization [21], which can be expressed as

$$f = c^2 = \left(F^{\mathrm{T}} U\right) \left(\overline{F^{\mathrm{T}} U}\right) \tag{5}$$

where $\overline{F^{\mathrm{T}} U}$ is the complex conjugate of $F^{\mathrm{T}} U$.

2.2 Optimization Formulation of Discrete Variable Topology Design

In this study, minimization of the square of structural dynamic compliance with the volume constraint is considered, and the corresponding optimization formulation based on discrete variables

can be expressed as follows:

Find : ρ

Min : $f(\rho) = c^2 = (F^T U)\left(\overline{F^T U}\right)$

S.t. :
$$\begin{cases} \left(K(\rho) - \omega^2 M(\rho) + i\omega C(\rho)\right) U = F \\ \dfrac{1}{N}\sum_{e=1}^{N} v_e \rho_e \leq \overline{V} \\ \rho_e \in \{0, 1\}, e = 1, 2, \ldots, N \end{cases} \tag{6}$$

where $\rho = [\rho_1, \rho_2, \ldots, \rho_N]$ is a set of design variables; N is the number of elements; v_e is the elemental volume; $\overline{V}$ denotes the predefined volume fraction.

The design variable in Eq. (6) is maintained as either 0 or 1, which allows material interpolation to be selected more flexibly because the intermediate densities need not necessarily be penalized. In fact, the material interpolation scheme of the present design is only for performing an efficient sensitivity analysis, which does not require an additional structural analysis. The global matrices K and M can be expressed as follows:

$$K(\rho) = \sum_{e=1}^{N}\left[E_{\min} + (E_0 - E_{\min})\rho_e^p K_e\right]$$

$$M(\rho) = \sum_{e=1}^{N}\left[E_{\min} + (E_0 - E_{\min})\rho_e^q M_e\right] \tag{7}$$

where K_e and M_e are elemental stiffness and mass matrices, respectively; $E_{\min}$ is an extremely low value to avoid singularity in the computation process. As demonstrated in the numerical examples, when the penalty coefficients are set as $p = 1$, $q = 1$ or $p = 3$, $q = 1$, 0–1 topology designs are achievable.

3 Discrete Variable Topology Optimization Based on SAIP

3.1 Subproblem of SAIP

The discrete variable optimization method transfers the large-scale implicit nonlinear integer programming of Eq. (6) into the following explicit sequential approximate integer programming subproblem (shown in Eq. (8)) based on the sensitivity of the discrete variable:

Find : ρ

Min : $\sum_{e=1}^{N} b_e \rho_e$

S.t. :
$$\begin{cases} \dfrac{1}{N}\sum_{e=1}^{N} v_e \rho_e \leq \overline{V} \\ \rho_e \in \{0, 1\}, e = 1, 2, \ldots, N \end{cases} \tag{8}$$

Here, b_e is the sensitivity of the discrete variable, which is defined as

$$b_e = \frac{\delta f}{\delta \rho_e} = \begin{cases} \dfrac{f(\rho_e = 1) - f\left(\rho_e^k = 0\right)}{1 - 0}, & \text{if} \quad \rho_e^k = 0 \\ \dfrac{f(\rho_e = 0) - f\left(\rho_e^k = 1\right)}{0 - 1}, & \text{if} \quad \rho_e^k = 1 \end{cases} \tag{9}$$

where ρ_e^k denotes the design variable of the current iteration. The discrete requirement of $\rho_e \in \{0, 1\}$ is equivalently transferred to the equality constraint $\rho_e (\rho_e - 1) = 0$. The equality and volume constraints are introduced into the Lagrange function, which is high-order differentiable and defined in Euclidean space. Subsequently, a smooth and differentiable dual function is constructed using first-order stability conditions [51]. Furthermore, an efficient CRA is employed to solve Eq. (8).

3.2 Sensitivity Analysis

Using the discrete variable sensitivity expressed in Eq. (9) incurs a significant amount of computational cost. To obtain the discrete variable sensitivity efficiently, the derivative of the objective function pertaining to the design variable can be expressed as

$$\frac{\delta f}{\delta \rho_e} \approx \frac{\partial f}{\partial \rho_e} = b_e = -2 \left(\overline{\boldsymbol{F}^{\mathrm{T}} \boldsymbol{U}} \right) \left(\boldsymbol{U}^{\mathrm{T}} \frac{\partial \boldsymbol{K}_d}{\partial \rho_e} \boldsymbol{U} \right) \tag{10}$$

where the equivalent stiffness matrix is

$$\boldsymbol{K}_d = \boldsymbol{K} - \omega^2 \boldsymbol{M} + i\omega \boldsymbol{C} \tag{11}$$

The derivative of $\boldsymbol{K}_d$ associated with the design variable can be calculated as follows:

$$\frac{\partial \boldsymbol{K}_d}{\partial \rho_e} = \frac{\partial \boldsymbol{K}}{\partial \rho_e} - \omega^2 \frac{\partial \boldsymbol{M}}{\partial \rho_e} + i\omega \frac{\partial \boldsymbol{C}}{\partial \rho_e} \tag{12}$$

where the derivative of $\boldsymbol{K}$ pertaining to the design variable can be calculated in the same manner as that presented in [51], as follows:

$$\frac{\partial \boldsymbol{K}}{\partial \rho_e} = \begin{cases} \rho_e (E_0 - E_{\min}) \boldsymbol{K}_e & \text{if} \quad p = 1 \\ p\rho_e^{p-1} (E_0 - E_{\min}) \boldsymbol{K}_e & \text{if} \quad p > 1 \end{cases} \tag{13}$$

and the derivative of $\boldsymbol{M}$ regarding to the design variable can be calculated by

$$\frac{\partial \boldsymbol{M}}{\partial \rho_e} = (E_0 - E_{\min}) \boldsymbol{M}_e \tag{14}$$

The proportional damping matrix $\boldsymbol{C}$ can be expressed as $\boldsymbol{C} = \alpha \boldsymbol{M} + \beta \boldsymbol{K}$, where α and β are the constant damping coefficients. The derivative of the damping matrix with respect to the design variable is expressed as

$$\frac{\partial \boldsymbol{C}}{\partial \rho_e} = \alpha \frac{\partial \boldsymbol{M}}{\partial \rho_e} + \beta \frac{\partial \boldsymbol{K}}{\partial \rho_e} \tag{15}$$

When $p > 1$, the sensitivity of the discrete variable is equal to that of the continuous variable. The sensitivity of the white element requires specific processing, as in Eq. (13), when $p = 1$ [52].

4 Geometrical Constraint for Minimum Length Scale Control

The optimization result of the topology design may contain thin bars, small holes, and sharp corners; thus, a geometrical constraint is utilized for size control [53]. If the length scale control of the material phase is satisfied, then it must be filled with the material (black), which is composed of a series of black disks with a specified radius. Similarly, if the length scale control of the void phase is satisfied, then the nonstructural zone must be filled with the void material (white), which is combined with a series of white-disks with a specified radius. Because the discrete variable method can achieve

a 0–1 topological design, the definition of the minimum length scale above can be directly utilized to formulate a valid geometrical constraint.

4.1 Geometrical Constraint Function

The locally averaged element density within a specified radius R is defined as

$$\widetilde{\rho}_e = \frac{\sum_{j\in N_e} v_j \rho_j}{\sum_{j\in N_e} v_j} \tag{16}$$

where ρ_j is a discrete design variable. Meanwhile, N_e is a set of element e at the specified radius R, which is defined as

$$N_e = \left\{ j \,\middle|\, |x_e - x_j| < \lceil R \rceil \text{ and } |y_e - y_j| < \lceil R \rceil \right\} \tag{17}$$

where (x_e, y_e) and (x_j, y_j) are the coordinates of the corresponding elemental center points. $\lceil R \rceil$ represents an integer rounded up to a specified radius R. Based on Eq. (17), N_e is a rectangular region. Because the finite element meshes used in this study are square meshes with unit size $l = 1$, the relationship between the minimum size radius $\widetilde{R}$ and the specified radius can be written as follows:

$$\widetilde{R} = \lceil R \rceil - \frac{1}{2}l = \lceil R \rceil - \frac{1}{2} \tag{18}$$

Because the design variable is discrete, the density at the structural boundary must change considerably such that the gradient value of the locally averaged density $||\nabla \widetilde{\rho}_e||_2^2$ can be utilized to distinguish the interior, exterior, and boundary of the structure. The following expressions are defined for the structural internal and external indicators:

$$I^I(\rho_e) = \rho_e \theta \left(||\nabla \widetilde{\rho}_e||_2^2 \right)$$

$$I^E(\rho_e) = (1 - \rho_e) \theta \left(||\nabla \widetilde{\rho}_e||_2^2 \right) \tag{19}$$

where $\theta(\cdot)$ is defined as

$$\theta \left(||\nabla \widetilde{\rho}_e||_2^2 \right) = \exp \left(-d ||\nabla \widetilde{\rho}_e||_2^2 \right) \tag{20}$$

Here, the minimum size of the material and void phases can be controlled by setting $d = R^2$. The central difference scheme is used to calculate the locally averaged density $||\nabla \widetilde{\rho}_e||_2^2$. If $\rho_e = 1$ and $||\nabla \widetilde{\rho}_e||_2^2 = 0$, then element e belongs to the interior of a structure, and $I^I(\rho_e) = 1$. By contrast, if $\rho_e = 0$ and $||\nabla \widetilde{\rho}_e||_2^2 = 0$, then element e belongs to the outside of a structure, and $I^E(\rho_e) = 1$.

To satisfy the requirement of minimum length scale control, the local average density inside the structure is set to 1, whereas the local average density outside the structure is set to 0. Hence, the following geometrical detection function can be constructed:

$$G^g(\boldsymbol{\rho}) = \sum_{e=1}^{N} \left[I^I(\rho_e)(1 - \widetilde{\rho}_e) + I^E(\rho_e)\widetilde{\rho}_e \right]$$

$$= \sum_{e=1}^{N} [\rho_e - 2\rho_e\widetilde{\rho}_e + \widetilde{\rho}_e] \theta \left(||\nabla \widetilde{\rho}_e||_2^2 \right) \tag{21}$$

However, the boundary elements are typically present in the structure. Even if the structure satisfies the size-control constraint, the value obtained using Eq. (21) cannot be completely equal to

zero; furthermore, it is significantly smaller than the corresponding value of the structure that violates the minimum length scale. Therefore, the geometrical constraint function is expressed as follows:

$$G^g(\boldsymbol{\rho}) = \sum_{e=1}^{N} \left[I^I(\rho_e)(1 - \widetilde{\rho}_e) + I^E(\rho_e)\widetilde{\rho}_e \right]$$

$$= \sum_{e=1}^{N} [\rho_e - 2\rho_e\widetilde{\rho}_e + \widetilde{\rho}_e]\theta\left(||\nabla\widetilde{\rho}_e||_2^2\right) \leq G^* \tag{22}$$

The right-end term G^* can be determined using the constraint relaxation strategy, as follows:

$$\hat{G}^g(\boldsymbol{\rho}) = \sum_{e=1}^{N} [\rho_e - 2\rho_e\widetilde{\rho}_e + \widetilde{\rho}_e]\theta\left(||\nabla\widetilde{\rho}_e||_2^2\right)$$

$$\leq G^g\left(\boldsymbol{\rho}^k\right) - \zeta G^g\left(\boldsymbol{\rho}^0\right) \tag{23}$$

where $\boldsymbol{\rho}^k$ is the design variable of the current iteration, and $\boldsymbol{\rho}^0$ is the initial design. ζ is an extremely small number and is set to 0.01. $\zeta G^g(\boldsymbol{\rho}^0)$ represents a reduction in the expected value of the geometrical constraint function in each iteration.

The nonlinear constraint in Eq. (23) can be linearized using the discrete variable sensitivity via a difference operation. The resulting integer programming problem with multiple constraints can be efficiently solved using the CRA.

The material layout and contribution terms are presented in Fig. 1. For $R = 4$ and 8, the material contribution terms in Eq. (21) are shown in Figs. 1a and 1b, respectively. As shown in the figures, slender rods, pointed hinges, small holes, and sharp corners that do not satisfy the requirement of the minimum size are identified. If the value of the geometric constraint function in Eq. (21) is reduced, then the topological details of the structure that do not satisfy minimum size control can be successfully eliminated.
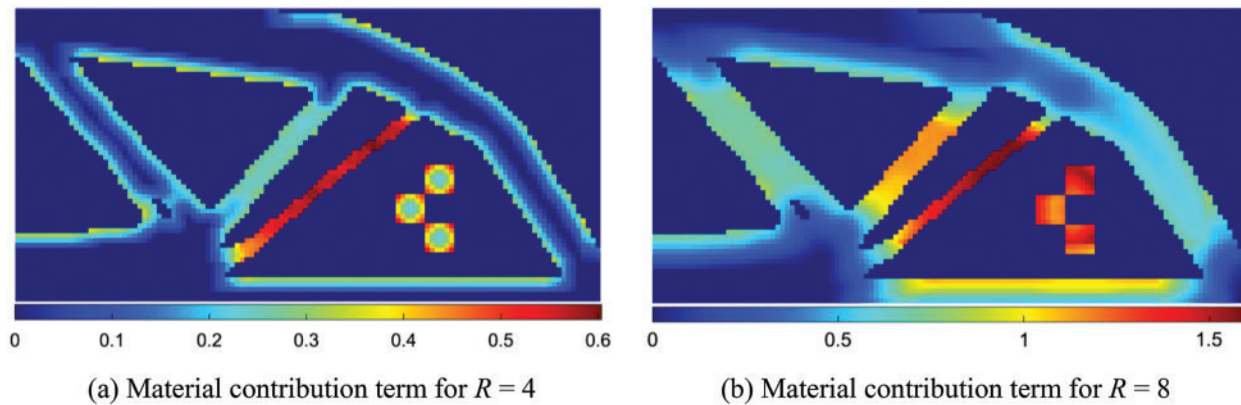

(a) Material contribution term for $R = 4$ (b) Material contribution term for $R = 8$

Figure 1: Material layout and material contribution term

4.2 Optimization Formulation of Minimum Length Scale Control

A relaxed linear constraint is applied to the minimum length scale control using the discrete variable sensitivity of the geometrical constraint function. Therefore, the SAIP subproblem of the topology design for harmonic excitation structures is formulated as

Find : $\boldsymbol{\rho}$

Min : $\sum\limits_{e=1}^{N} b_e \rho_e$

(24)

S.t. : $\begin{cases} \dfrac{1}{N} \sum\limits_{e=1}^{N} v_e \rho_e \leq \overline{V} \\ \overline{G}^g (\boldsymbol{\rho}) = G^g (\boldsymbol{\rho}^k) + \sum\limits_{i=1}^{N} \dfrac{\delta G^g}{\delta \rho_e} (\rho_e - \rho_e^k) \\ \leq G^g (\boldsymbol{\rho}^k) - \zeta G^g (\boldsymbol{\rho}^0) \\ \rho_e \in \{0, 1\}, e = 1, 2, \ldots, N \end{cases}$

The CRA is employed to solve the optimization problem expressed in Eq. (24) until the variations of the adjacent objective function and constraint function are less than the specified tolerance, thus resulting in design results that fulfill the minimum length scale requirement. Accordingly, the flowchart of harmonic excitation topology optimization with minimum length scale control based on the discrete variable method is shown in Fig. 2.
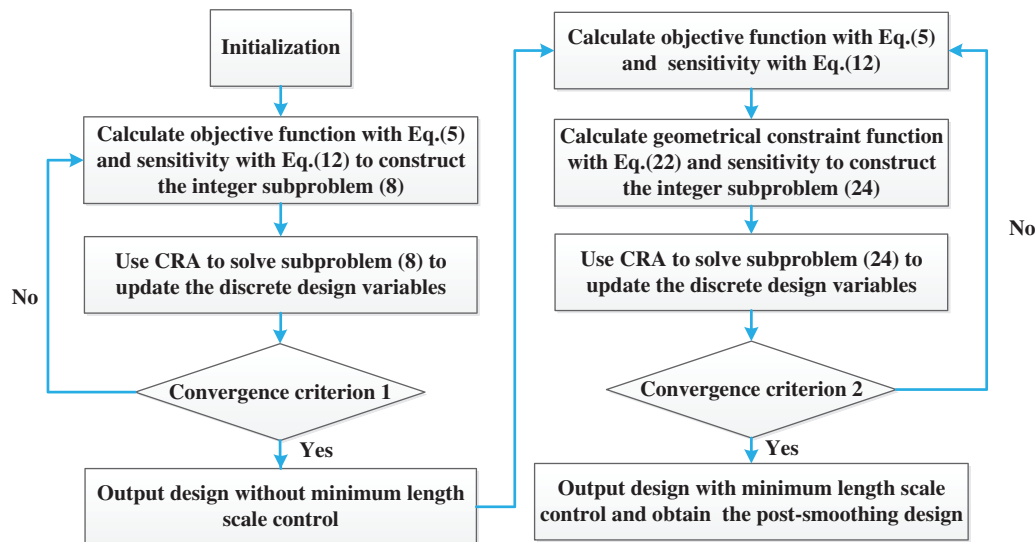
Figure 2: The procedure flowchart

5 Symmetry of Optimal Design under Harmonic Excitation

The optimal solution of the static problem must be symmetric when the load and support are symmetric. For frame topology optimization with the constraint of fundamental frequency, the optimal solution can be asymmetric, even when the geometry, material distribution, and structure are symmetric [48]. Guo et al. [49] employed group theory to investigate the symmetry problem of structural optimization, including static compliance optimization and fundamental frequency optimization. However, the symmetry results for harmonic excitation topology optimization were not presented, and the specific reason for the asymmetric solution was not divulged. In this section, we prove that the optimal solution of the harmonic excitation problem may be asymmetrical even when the load and support are symmetric. In this regard, the three-bar truss problem, as illustrated in Fig. 3, is investigated.
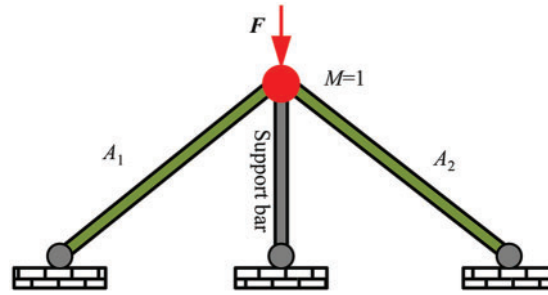
Figure 3: The three-bar truss structure

The design variables are the cross-sectional areas of the members, namely A_1 and A_2. The members are assumed to contribute only to the stiffness and not the mass, and a concentrated mass exists at the degree-of-freedom position with a magnitude of 1, and the Young's modulus is unity. The corresponding stiffness and mass matrices are expressed as follows:

$$K(A_1, A_2) = \begin{bmatrix} A_1 + A_2 + 1 & A_2 - A_1 \\ A_2 - A_1 & A_1 + A_2 \end{bmatrix}$$

$$M(A_1, A_2) = \begin{bmatrix} 1 & 0 \\ 0 & 1 \end{bmatrix}$$

(25)

This model was utilized to investigate the symmetry problem of fundamental frequency optimization in [50]. In this study, the model is employed to discuss the symmetry problem of structural topology optimization under harmonic excitation. The external harmonic vibration load is set as follows:

$$F = \begin{bmatrix} F_1 \\ F_2 \end{bmatrix} = \begin{bmatrix} 0 \\ 1 \end{bmatrix}$$

(26)

Assuming that damping is not considered tentatively, the optimization formulation for the minimum dynamic compliance with a specified amount of material can be written as

$$\text{Min}: \quad C_d(A_1, A_2, U) = \left(F^{\mathrm{T}} U\right) \left(\overline{F^{\mathrm{T}} U}\right)$$

$$\text{S.t.}: \quad \begin{cases} \begin{bmatrix} A_1 + A_2 + 1 - \omega^2 & A_2 - A_1 \\ A_2 - A_1 & A_1 + A_2 - \omega^2 \end{bmatrix} \begin{bmatrix} U_1 \\ U_2 \end{bmatrix} = \begin{bmatrix} 0 \\ 1 \end{bmatrix} \\ A_1 + A_2 = 1, \quad A_1 \text{ and } A_2 \in [0, 1] \end{cases}$$

(27)

The variable is specified as a continuous variable. Owing to the absence of damping, the objective function is expressed as

$$C_d(A_1, A_2, U) = U_2 \cdot \overline{U_2}$$

(28)

Based on Eq. (27), it can be expressed as

$$\begin{bmatrix} A_1 + A_2 + 1 - \omega^2 & A_2 - A_1 \\ A_2 - A_1 & A_1 + A_2 - \omega^2 \end{bmatrix} \begin{bmatrix} U_1 \\ U_2 \end{bmatrix} = \begin{bmatrix} 0 \\ 1 \end{bmatrix}$$

$$\Rightarrow \begin{bmatrix} U_1 \\ U_2 \end{bmatrix} = \begin{bmatrix} A_1 + A_2 + 1 - \omega^2 & A_2 - A_1 \\ A_2 - A_1 & A_1 + A_2 - \omega^2 \end{bmatrix}^{-1} \begin{bmatrix} 0 \\ 1 \end{bmatrix}$$

$$\Rightarrow \begin{bmatrix} U_1 \\ U_2 \end{bmatrix} = \frac{1}{(A_1 + A_2 + 1 - \omega^2)(A_1 + A_2 - \omega^2) - (A_1 - A_2)^2} \begin{bmatrix} A_1 - A_2 \\ A_1 + A_2 + 1 - \omega^2 \end{bmatrix} \tag{29}$$

The dynamic compliance can be written as

$$C_d(A_1, A_2, \boldsymbol{U}) = U_2 \cdot \overline{U_2}$$

$$= \left(\frac{A_1 + A_2 + 1 - \omega^2}{(A_1 + A_2 + 1 - \omega^2)(A_1 + A_2 - \omega^2) - (A_1 - A_2)^2} \right)^2 \tag{30}$$

Subsequently, it can be transformed into the following explicit quasi-unconstrained optimization problem:

$$\text{Min}: \quad C_d(A_2) = \left(\frac{2 - \omega^2}{(2 - \omega^2)(1 - \omega^2) - (2A_2 - 1)^2} \right)^2 \tag{31}$$

S.t. : $\quad A_1, A_2 \in [0, 1]$

The convexity of the explicit optimization problem under various external load frequencies is analyzed herein. To facilitate the derivation, we set $a = \omega^2$. The first and second derivatives of the dynamic compliance are expressed as follows:

$$\frac{dC_d}{dA_2} = \frac{-2(8A_2 - 4)(a - 2)^2}{\left[(2A_2 - 1)^2 - (a - 1)(a - 2)\right]^3}$$

$$\frac{d^2 C_d}{d(A_2)^2} = \frac{6(8A_2 - 4)^2(a - 2)^2}{\left[(2A_2 - 1)^2 - (a - 1)(a - 2)\right]^4} - \frac{16(a - 2)^2}{\left[(2A_2 - 1)^2 - (a - 1)(a - 2)\right]^3} \tag{32}$$

Next, we explain that if the second derivative of the dynamic compliance is positive under the condition $a = \omega^2$, then the original optimization problem is convex and a symmetric optimal solution exists [50]. Otherwise, the optimal solution may be asymmetrical. Based on the convexity requirement, the following nonlinear inequality equation is solved:

$$\text{Find } a = \omega^2, \forall A_2 \in [0, 1], \frac{d^2 C_d}{d(A_2)^2} \geq 0 \tag{33}$$

Eq. (33) can be described based on the following two conditions:

Condition I : $\forall A_2 \in [0, 1]$,

$$\left[(2A_2 - 1)^2 - (a - 1)(a - 2)\right] \neq 0 \tag{34a}$$

Condition II : $\forall A_2 \in [0, 1]$,

$$\left[6(8A_2 - 4)^2\right] \geq \left[16(2A_2 - 1)^2 - 16(a - 1)(a - 2)\right] \tag{34b}$$

According to Condition I, $\forall A_2 \in [0, 1], a^2 - 3a + 2 \neq (2A_2 - 1)^2$. Thus, the range of $(2A_2 - 1)^2$ is $[0, 1]$. Subsequently, the following can be obtained:

$$a = \omega^2 < \frac{3 - \sqrt{5}}{2} \text{ or } a = \omega^2 > \frac{3 + \sqrt{5}}{2} \tag{35}$$

According to Condition II, $\forall A_2 \in [0, 1], -a^2 + 3a \leq 20A_2^2 - 20A_2 + 7$, namely $\forall A_2 \in [0, 1], -a^2 + 3a \leq \min_{A_2 \in [0,1]} \left[20A_2^2 - 20A_2 + 7\right]$. Therefore, the minimum value is obtained when $A_2 = 0.5$, and

Condition II can be further derived as

$$-a^2 + 3a \leq 2 \Rightarrow (a-1)(a-2) \geq 0$$
$$\Rightarrow \omega^2 \leq 1 \text{ or } \omega^2 \geq 2 \tag{36}$$

Based on Eqs. (35) and (36), the following conclusions can be inferred:

(1) When $\omega^2 < \dfrac{3-\sqrt{5}}{2}$, the present harmonic vibration optimization problem is convex, and the symmetric design $(A_1, A_2) = (0.5, 0.5)$ is a locally and globally optimal solution.

(2) When $\dfrac{3-\sqrt{5}}{2} \leq \omega^2 < 1$, the optimization problem is not convex, and the symmetric design $(A_1, A_2) = (0.5, 0.5)$ is a locally optimal solution (the first-order stability condition and second-order positive definite conditions are satisfied).

(3) When $1 \leq \omega^2 < 2$, the optimization problem is not convex. Furthermore, the symmetric design $(A_1, A_2) = (0.5, 0.5)$ is not a locally optimal solution, and the maximum value of the dynamic compliance may be achieved (the first-order stability condition is satisfied, whereas the second-order positive definite condition is not satisfied).

(4) When $2 < \omega^2 < \dfrac{3+\sqrt{5}}{2}$, the optimization problem is not convex. However, the symmetric design $(A_1, A_2) = (0.5, 0.5)$ is a locally optimal solution (the first-order stability condition and second-order positive definite conditions are satisfied).

(5) When $\omega^2 \geq \dfrac{3+\sqrt{5}}{2}$, the present harmonic vibration optimization problem is convex, and the symmetric design $(A_1, A_2) = (0.5, 0.5)$ is a locally and globally optimal solution.

To further illustrate the conclusions above, the curves of dynamic compliance change with the design variable A_2 under different external load frequencies are depicted.

(a) The corresponding relationship curve for an external load frequency ω^2 of 0.3 is shown in Fig. 4. Based on the curve, the optimization problem is a convex optimization problem, and the symmetric solution is the globally optimal solution.
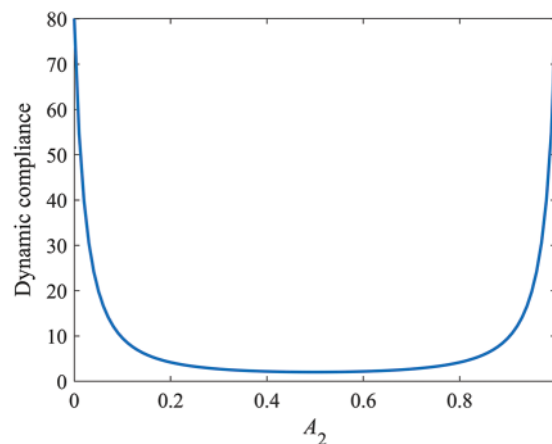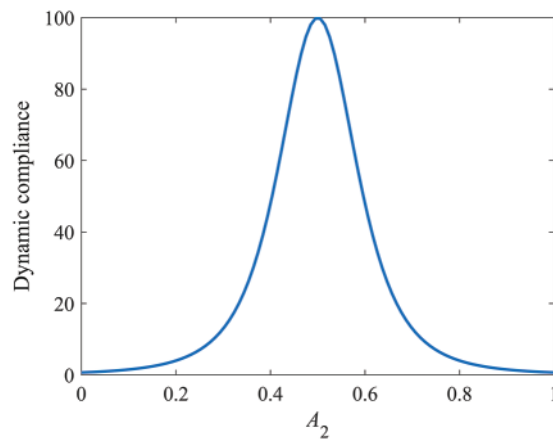

Figure 4: Relationship curve of $\omega^2 = 0.3$

(b) When the external load frequency ω^2 is 0.5, the corresponding relationship curve is as depicted in Fig. 5. Because of the nonconvex nature of the optimization problem, two resonance peaks emerged when the design variables are 0.07 and 0.93. The symmetric solution is the locally optimal solution, and it remains the globally optimal solution in terms of dynamic compliance.

(c) When the external load frequency ω^2 is 1.1, the corresponding relationship curve is as shown in Fig. 6. In this case, the symmetric design is not a locally optimal solution but achieves the maximum dynamic compliance. In this case, the globally optimal solution is $(A_1, A_2) = (1, 0)$ or $(0, 1)$, which is an asymmetric design.
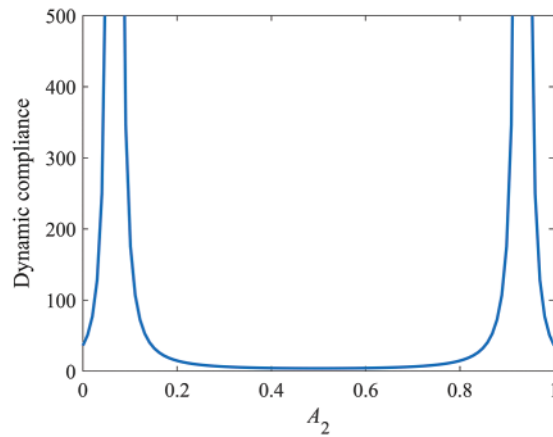
Figure 5: Relationship curve of $\omega^2 = 0.5$

Figure 6: Relationship curve of $\omega^2 = 1.1$

(d) When the external load frequency ω^2 is 2.1, the corresponding relationship curve is as shown in Fig. 7. In this case, two resonance peaks emerged. The optimization problem is nonconvex, and the symmetric solution is a locally optimal solution.
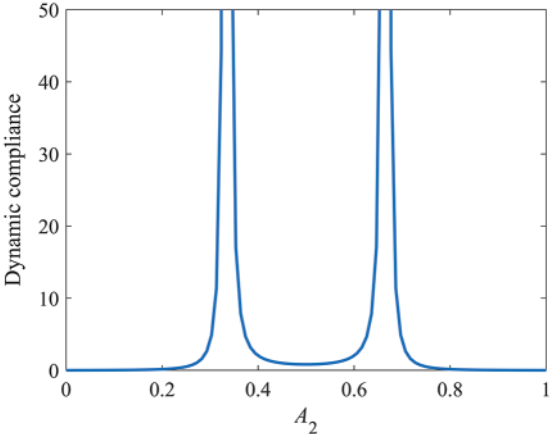
Figure 7: Relationship curve of $\omega^2 = 2.1$

(e) When the external load frequency ω^2 is equals to 3, the corresponding relationship curve is as shown in Fig. 8. In this case, the optimization problem is convex, and the symmetric solution is a globally optimal solution.
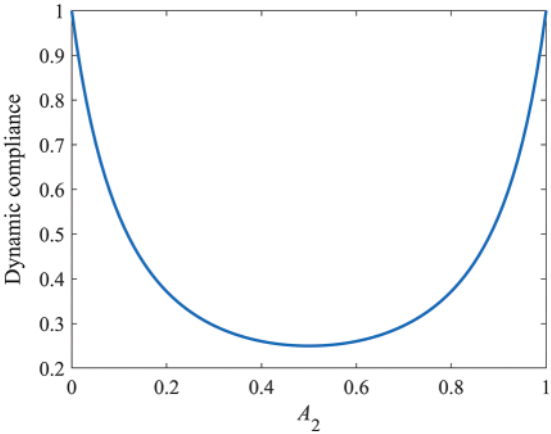

Figure 8: Relationship curve of $\omega^2 = 3$

In conclusion, the optimal solution of structural topology optimization under harmonic excitation may be asymmetric even when the load and support are symmetric. When the excitation frequency exceeds a certain value, the symmetric design may achieve the maximum dynamic compliance, which implies an inferior design. Therefore, unlike the static optimization problem, one-half of the design area cannot be selected for calculation based on the load and support symmetry in harmonic excitation topology optimization, which will be further discussed in the next section.

6 Numerical Examples

In this section, several numerical examples are presented to demonstrate the effectiveness of the discrete variable topology design under harmonic excitation and the geometrical constraint method. The load is $F = 100e^{i\omega t}$ N. The Young's modulus (E), Poisson's ratio (v), and mass density of the solid

material are 2.1×10^5 MPa, 0.3, and $7800\,\mathrm{kg/m^3}$, respectively. The proportional damping coefficients are set as $\alpha = 5.24 \times 10^{-1}$ and $\beta = 1.63 \times 10^{-7}$. The limit of the structural volume is $\overline{V} = 0.5$. A sensitivity filtering technique is employed to suppress checkerboard instability [42]. The convergence criterion of the discrete variable design is that the relative change of dynamic compliance is less than 5×10^{-3}. Additionally, c^2 and N_{step} are the objective function value and total iteration number of the optimized design, respectively. G represents the value of the geometric constraint function.

6.1 MBB Beam

First, the topological design of the MBB beam structure, as shown in Fig. 9, is considered. The first resonant frequency is 1556 Hz, and the excitation frequencies are specified as 50, 500, and 1450 Hz. The structure is discretized using 240×60 bilinear finite elements with four nodes. The filtering radius is set as $r_{\mathrm{min}} = 2$. For comparison, density-based SIMP designs are presented. Notably, many gray regions and fuzzy boundaries appear in SIMP-based designs when the objective function value converges. Therefore, a constant iteration number of 300 is used for the SIMP-based designs. For an unbiased comparison, the initial designs for both the discrete variable and SIMP methods are based on full materials. The typically used initial designs in the SIMP method are the targeted volume fractions. However, the allowable excitation frequency must be decreased considerably because the first resonance frequency of the initial design is relatively low. Additionally, the initial design of the SIMP method based on a full material may incur additional numerical costs.
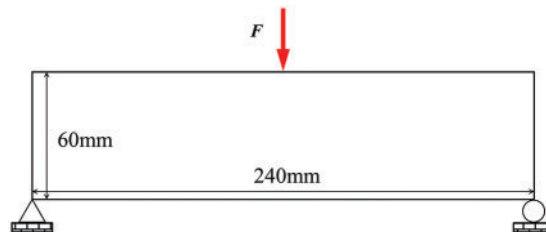

Figure 9: The MBB beam structure

The discrete variable and SIMP-based designs based on $\omega = 50$ Hz are shown in Fig. 10. Evidently, a 0–1 topology design is achieved when the discrete variable method is used, and the iterative number (N_{step}) is 90 when the convergence criterion is used. The statistical results for the non-integer variables are shown in Table 1, where N_{NIV} denotes the number of non-integer variables, and "rat" denotes the ratio of the number of non-integer variables to the total number of design variables. The total number of design variables is 14400. Additionally, non-integer variables are few; thus, the rounding operation is employed to achieve an integer solution. This simple post-processing method does not significantly affect the topology design.
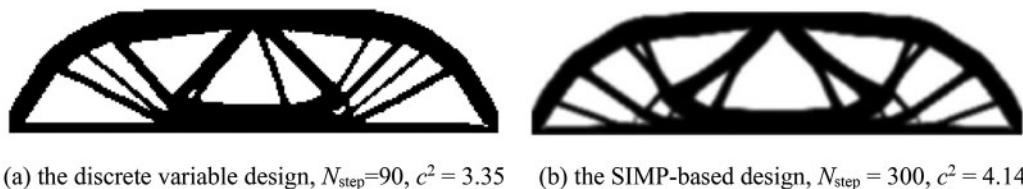

(a) the discrete variable design, N_{step}=90, $c^2 = 3.35$ (b) the SIMP-based design, $N_{\mathrm{step}} = 300$, $c^2 = 4.14$

Figure 10: Topology design of the MBB beam, $\omega = 50$ Hz

Table 1: Statistical results for the non-integer variables

Volume fraction	$0.01 \leq \rho_e \leq 0.99$	$\rho_e \geq 1.01$	$\rho_e \leq -0.01$
0.80	rat $= 6.2500\mathrm{e}{-04}$	rat $= 1.3889\mathrm{e}{-04}$	rat $= 0$
	$N_{\mathrm{NIV}} = 9$	$N_{\mathrm{NIV}} = 2$	$N_{\mathrm{NIV}} = 0$
0.50	rat $= 0$	rat $= 3.4722\mathrm{e}{-04}$	rat $= 3.4722\mathrm{e}{-04}$
	$N_{\mathrm{NIV}} = 0$	$N_{\mathrm{NIV}} = 5$	$N_{\mathrm{NIV}} = 5$

By contrast, gray regions and fuzzy boundaries appear in the SIMP-based design, even though the iterative number is set to 300. The discrete variable design can avoid spurious vibration modes naturally; however, it must be deliberately addressed for SIMP-based designs, as presented in [40]. In addition, the discrete variable design shown in Fig. 10a is asymmetric, whereas the SIMP-based design presented in Fig. 10b is symmetric. The optimal topology designs of the two methods ($\omega = 500\,\mathrm{Hz}$) are shown in Fig. 11. When the excitation frequency is increased, the asymmetry of the discrete variable design is more evident, and the SIMP-based design becomes asymmetrical. Based on Figs. 10 and 11, the discrete variable designs are improved by approximately 23% as compared with the SIMP-based designs.
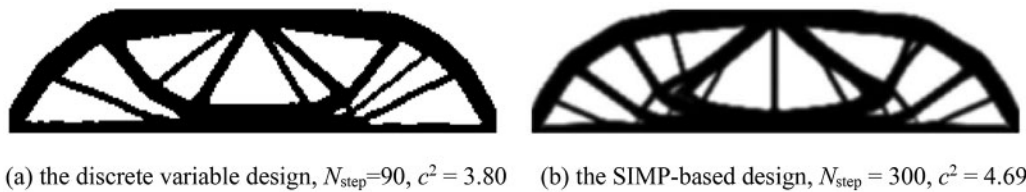

(a) the discrete variable design, N_{step}=90, $c^2 = 3.80$ (b) the SIMP-based design, $N_{\mathrm{step}} = 300$, $c^2 = 4.69$

Figure 11: Topology design of the MBB beam, $\omega = 500\,\mathrm{Hz}$

For the SIMP-based design, the measurement of the 0–1 level is expressed as [57]

$$GR = \frac{\sum_{i=1}^{N_m} \rho_i}{N_m}, \rho_i > \rho_{\min} \tag{37}$$

where $\rho_{\min}$ is set to 0.005, and N_m is the number of elemental densities exceeding $\rho_{\min}$. When $GR = 1$, the structure exhibits an all-black design, whereas when $GR = 0$, it exhibits an all-white design.

The optimal designs of the discrete variable method based on $\omega = 1450\,\mathrm{Hz}$ are shown in Fig. 12. The objective value is 12.29, and the design solution is asymmetrical. The optimal topology design obtained using the symmetric boundary condition is shown in Fig. 13, and the objective value is 13.86. By considering the structural symmetry, only one-half of the structure is to be calculated for topology optimization. It is evident that the objective value of the design result shown in Fig. 12 is better than that presented in Fig. 13. The SIMP design based on $\omega = 1450\,\mathrm{Hz}$ is shown in Fig. 14, which is significantly different from the optimized configuration of the SAIP method shown in Fig. 12. The frequency-response curves are shown in Fig. 15. As shown, the first resonant frequencies of the optimized results are improved, and the asymmetrical design performs better than the symmetric design by 6%. Notably, if the initial SIMP design features intermediate densities, then structural design optimization based on $\omega = 1450\,\mathrm{Hz}$ cannot be implemented. However, the initial SIMP design of the full material will increase the number of computational iterations, as shown by the grayscale index in Fig. 16; this implies that more iterations are required in the SIMP method to penalize the

intermediate densities and achieve the 0–1 design after a fuzzy topology configuration is obtained. Based on Figs. 15 and 16, when a relatively high excitation frequency is considered in the present discrete variable optimization, the design iteration is stable within 100 steps, and a faster convergence can be achieved. Furthermore, the first resonance frequency of the optimization result is improved significantly; thus, the discrete variable design can avoid resonance over a wider range of excitation frequencies. Meanwhile, the localized vibration modes can be avoided naturally. Therefore, the present discrete variable method can efficiently achieve a 0–1 optimum design with an improved resonance frequency over a wide range of excitation frequencies.

Figure 12: Discrete variable design with $\omega = 1450$ Hz, $N_{step} = 103$, $c^2 = 12.29$

Figure 13: Discrete variable design utilizing the symmetric boundary condition, $N_{step} = 97$, $c^2 = 13.86$, $\omega = 1450$ Hz

Figure 14: SIMP design with $\omega = 1450$ Hz, $N_{step} = 300$, $c^2 = 18.47$
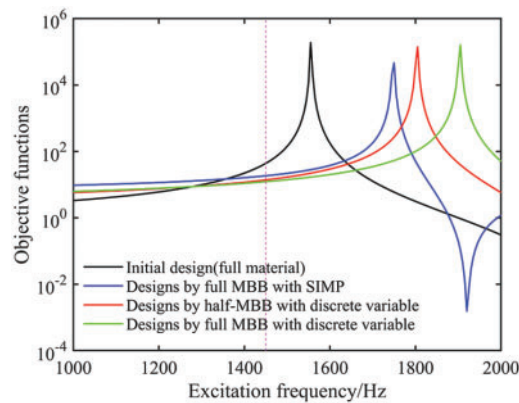

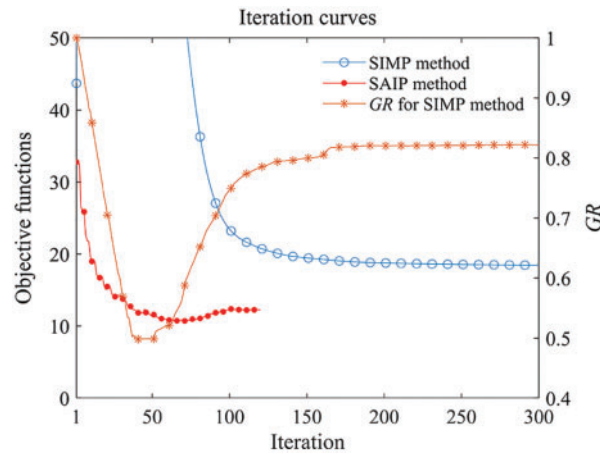**Figure 15:** Frequency response curves

Figure 16: Iterative curves for the SAIP and the SIMP method

6.2 Clamped–Clamped Beam

A clamped–clamped beam, as shown in Fig. 17, is considered in this study. Its excitation frequency ω and filtering radius r_{min} are 50 Hz and 2, respectively. Furthermore, it is discretized by using 240×40 bilinear finite elements with four nodes.
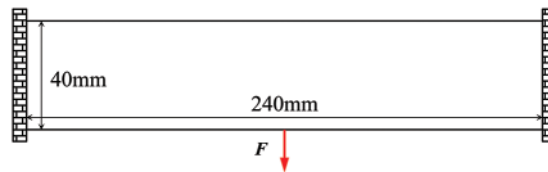

Figure 17: A clamped-clamped beam structure

In the optimal topology design of the clamped–clamped beam, as shown in Fig. 18, the penalty coefficient is set as $p = 3$, and the objective value is 2.74. The topological design based on the discrete variable method by setting the penalty coefficient to $p = 1$ is shown in Fig. 19. When the penalty coefficient is set to 1, the discrete variable method can still achieve a black-and-white design with distinct topology. As shown in Fig. 20, the discrete variable designs of the intermediate volume fraction are also available designs, i.e., all the topology designs from the initial design to the predefined volume ratio (Pareto frontier) can be achieved in one optimization solution. When the excitation frequency is relatively high (approximately the first resonance frequency of the initial design) and the volume ratio is equal to 0.7, more materials are concentrated at the fixed supports, which increase the stiffness and weaken the inertia effect, as shown in Fig. 21, thus reflecting the dynamic effect of topology optimization while considering harmonic excitation.

Figure 18: The discrete variable design of the clamped-clamped beam, $N_{step} = 93$, $p = 3$, $c^2 = 2.74$

Figure 19: The discrete variable design of the clamped-clamped beam, $N_{step} = 93$, $p = 1$, $c^2 = 2.82$
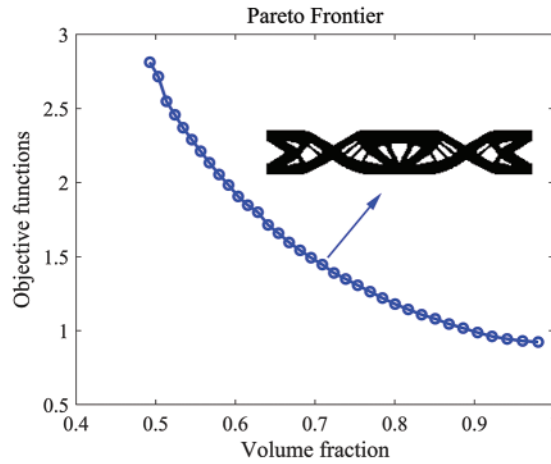

Figure 20: Pareto frontier, where the average number of finite element analysis for each Pareto frontier point is 93/35

Figure 21: The discrete variable design of the clamped-clamped beam with a relatively high excitation frequency

6.3 Cantilever Beam

In this subsection, the topological design of the cantilever beam structure, as shown in Fig. 22, is discussed. Its excitation frequency is $\omega = 50\,\text{Hz}$, and 120×60 bilinear finite elements with four nodes are adopted.
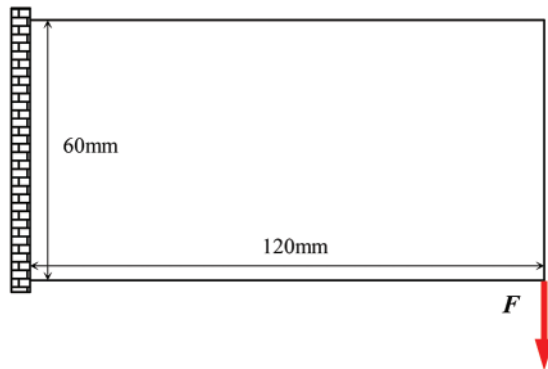

Figure 22: A cantilever beam structure

The optimal topology designs of the present discrete variable method are shown in Fig. 23, where the sensitivity filtering radii are set as 2, 3, 4 and 5. As the filtering radius increases, finer structures are gradually filtered out, and the objective value increases. The filtering radius size can affect the optimal design configuration; additionally, it can be used to indirectly control the feature size to avoid mesh dependence. As shown in Fig. 23a, the optimization result contains thin bars, small holes, and sharp corners when the filter radius is small, whereas the optimization result still contains sharp corners when the filter radius is relatively large, as shown in Fig. 23d. Thus, a geometrical constraint for size control is employed, where the sensitivity filtering radius and specified radius R are set to 2 and 6, respectively. The optimal design is shown in the third column of the first row of Table 2; it can eliminate thin bars, small holes, and sharp corners, thus improving the manufacturability of the structural design.
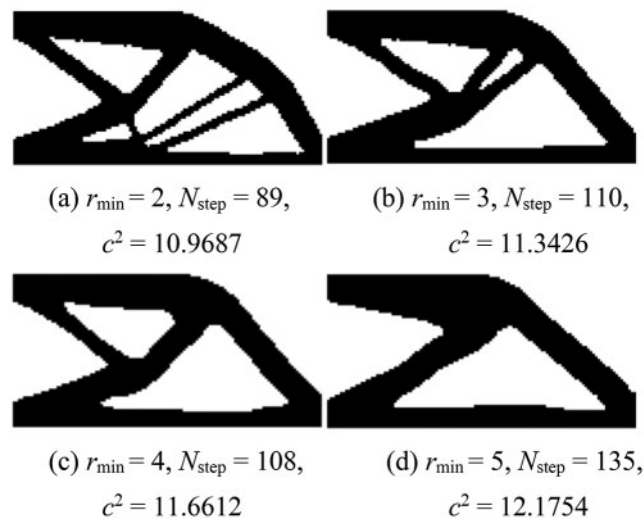

(a) $r_{min} = 2$, $N_{step} = 89$, $c^2 = 10.9687$

(b) $r_{min} = 3$, $N_{step} = 110$, $c^2 = 11.3426$

(c) $r_{min} = 4$, $N_{step} = 108$, $c^2 = 11.6612$

(d) $r_{min} = 5$, $N_{step} = 135$, $c^2 = 12.1754$

Figure 23: The discrete variable designs of the cantilever beam

Subsequently, two different finite element meshes (120×60 and 180×90) are considered. The corresponding filter radii are 2 and 3, and the radii R of the size control are set to 6 and 9, respectively. The topology design results are presented in Table 2. For the two mesh refinements, the ratio of the filter radius r_{min} to the number of meshes is the same, namely $2/120 = 3/180$. The ratio of the specified control radius R to the number of meshes is the same as well, i.e., $6/120 = 9/180$. This implies that the mesh-dependent designs are further optimized into mesh-independent designs that fulfill the requirement of the minimum length scale. The post-smoothing design is shown in Table 2, which is able to get the nodal density based on the elemental density, and the level set function is obtained via linear interpolation within the element based on the nodal density. The threshold of the level set is determined via dichotomy to ensure that the volume of the level set function (greater than zero) is equal to the volume constraint. Because discrete variable designs feature a 0–1 topology configuration and clear boundaries, post-smoothing will not significantly affect the objective function. Furthermore, the loss of the objective value for the smooth design is less significant when additional size control is applied. Thus, the smooth designs in Table 2 that satisfy the minimum size requirements are more convenient for the manufacturing. For example, the design can be manufactured via a machining technique where the minimum length scale is strictly restricted by the size of the machining drill [40].

Table 2: Topology designs achieved by two different finite element meshes

Mesh	Initial topology design	Topology design with the minimum length scale control
(120×60)	$c^2 = 10.9687$, $G = 649.9486$, $r_{min} = 2$ $c^2 = 11.4234$	$c^2 = 12.0101$, $G = 312.9967$, $R = 2$ $c^2 = 12.2952$
(180×90)	$c^2 = 11.3294$, $G = 1278.4$, $r_{min} = 3$ $c^2 = 11.5670$	$c^2 = 12.2962$, $G = 730.5809$, $R = 9$ $c^2 = 12.4638$

7 Conclusions

In this study, the discrete variable design method is employed to perform topology design optimization under harmonic excitation. To satisfy the size control constraints in the manufacturing process, minimum length scale control is transformed into geometrical constraints and solved efficiently using the optimization framework presented herein. Subsequently, the topological design model and sensitivity formulation are derived. Compared with the solution of the classical statics problem, the optimal solution of the harmonic excitation structure is not necessarily symmetric when the load and support are symmetric. Thus, one-half of the design domain cannot be selected based on the load and support symmetry. The discrete variable method can efficiently achieve a 0–1 topology design with an improved resonance frequency over a wide range of excitation frequencies. Using the geometrical constraint for the minimum length scale control, the mesh dependence of the topology design optimization is effectively addressed, and thin bars, small holes, and sharp corners are eliminated, which improves the manufacturability of the structural design.

The geometrical constraint for the minimum length scale control only requires a calculation of the average density and average density gradient within a specified size range to be applied to the complex structure. For complex meshes, Helmholtz filtering can be utilized to efficiently calculate the local average density by solving partial differential equations, and the technique proposed by Crispo et al. [58] can be used to calculate spatial gradients. Studies will be performed in the future to identify a new method to address the minimum length scale control of engineering structure designs with complex meshes. Furthermore, the sampling points in the frequency range yield numerous finite

element equations of state with different coefficients, which incur high computational costs. This issue shall be addressed in future studies. The results of this study can provide a basis for structural optimization under harmonic excitation in the frequency range, since the potential of the present algorithm for solving dynamic optimization problems is confirmed.

Conflicts of Interest: The authors declare that they have no conflicts of interest to report regarding the present study.

References

1. Sigmund, O., Maute, K. (2013). Topology optimization approaches. *Structural and Multidisciplinary Optimization, 48(6),* 1031–1055. DOI 10.1007/s00158-013-0978-6.

2. Deaton, J. D., Grandhi, R. V. (2014). A survey of structural and multidisciplinary continuum topology optimization: Post 2000. *Structural and Multidisciplinary Optimization, 49(1),* 1–38. DOI 10.1007/s00158-013-0956-z.

3. Bendsøe, M. P., Kikuchi, N. (1988). Generating optimal topologies in structural design using a homogenization method. *Computer Methods in Applied Mechanics & Engineering, 71(2),* 197–224. DOI 10.1016/0045-7825(88)90086-2.

4. Bendsøe, M. P., Sigmund, O. (2003). *Topology optimization: Theory, methods and applications.* Berlin: Springer.

5. Yan, J., Sui, Q., Fan, Z., Duan, Z. (2022). Multi-material and multiscale topology design optimization of thermoelastic lattice structures. *Computer Modeling in Engineering & Sciences, 130(2),* 967–986. DOI 10.32604/cmes.2022.017708.

6. Lee, C., Natarajan, S., Kee, S., Yee, J. (2022). A Cell-based linear smoothed finite element method for polygonal topology optimization. *Computer Modeling in Engineering & Sciences, 131(3),* 1615–1634. DOI 10.32604/cmes.2022.020377.

7. Xie, Y. M., Steven, G. P. (1993). A simple evolutionary procedure for structural optimization. *Computers Structures, 49(5),* 885–896. DOI 10.1016/0045-7949(93)90035-C.

8. Ye, H. L., Yuan, B. S., Li, J. C., Zhang, X., Sui, Y. K. (2021). Geometrically nonlinear topology optimization of continuum structures based on an independent continuous mapping method. *Acta Mechanica Solida Sinica, 34(5),* 658–672. DOI 10.1007/s10338-021-00229-9.

9. Wang, M. Y., Wang, X., Guo, D. M. (2003). A level set method for structural topology optimization. *Computer Methods in Applied Mechanics Engineering, 192,* 227–246. DOI 10.1016/S0045-7825(02)00559-5.

10. Allaire, G., Jouve, F., Toader, A. M. (2004). Structural optimization using sensitivity analysis and a level-set method. *Journal of Computational Physics, 194(1),* 363–393. DOI 10.1016/j.jcp.2003.09.032.

11. Cui, T., Du, Z., Liu, C., Sun, Z., Guo, X. (2022). Explicit topology optimization with moving morphable component (MMC) introduction mechanism. *Acta Mechanica Solida Sinica, 35,* 384–408. DOI 10.1007/s10338-021-00308-x.

12. Zhou, Y., Zhang, W. H., Zhu, J. H., Xu, Z. (2016). Feature-driven topology optimization method with signed distance function. *Computer Methods in Applied Mechanics Engineering, 310,* 1–32. DOI 10.1016/j.cma.2016.06.027.

13. Ma, L., Zhang, W., Cai, S. C., Li, S. (2021). The dynamic amplification factors for continuous beam bridges along high-speed railways. *Advances in Structural Engineering, 24(11),* 2542–2554. DOI 10.1177/13694332211003288.

14. Ma, L., Wu, L., Cai, C. S., Li, S. (2021). The theoretical impact factor spectrum for highway beam bridges. *Journal of Bridge Engineering, 26(12),* 04021089. DOI 10.1061/(ASCE)BE.1943-5592.0001800.

15. Gao, J., Luo, Z., Li, H., Li, P. G., Gao, L. (2019). Dynamic multiscale topology optimization for multi-regional micro-structured cellular composites. *Composite Structures, 211,* 401–417. DOI 10.1016/j.compstruct.2018.12.031.

16. Montero, D. S., Silva, O. M., Cardoso, E. L. (2020). Topology optimization for harmonic vibration problems using a density-weighted norm objective function. *Structural and Multidisciplinary Optimization, 62,* 3301–3327. DOI 10.1007/s00158-020-02695-0.

17. Liu, H., Zhang, W. H., Zhu, J. H. (2013). Structural topology optimization and frequency influence analysis under harmonic force excitations. *Chinese Journal of Theoretical and Applied Mechanics, 45,* 588–597. DOI 10.6052/0459-1879-12-253.

18. Liu, B., Huang, X. D., Huang, C. F., Sun, G. Y., Yan, X. L. et al. (2017). Topological design of structures under dynamic periodic loads. *Engineering Structures, 142(1),* 128–136. DOI 10.1016/j.engstruct.2017.03.067.

19. Niu, B., He, X., Shan, Y., Yang, R. (2018). On objective functions of minimizing the vibration response of continuum structures subjected to external harmonic excitation. *Structural and Multidisciplinary Optimization, 57,* 2291–2307. DOI 10.1007/s00158-017-1859-1.

20. Zhou, E. L., Wu, Y., Lin, X. Y., Li, Q. Q., Xiang, Y. (2021). A normalization strategy for BESO-based structural optimization and its application to frequency response suppression. *Acta Mechanica, 232,* 1307–1327. DOI 10.1007/s00707-020-02862-w.

21. Olhoff, N., Du, J. (2016). Generalized incremental frequency method for topological design of continuum structures for minimum dynamic compliance subject to forced vibration at a prescribed low or high value of the excitation frequency. *Structural and Multidisciplinary Optimization, 54,* 1113–1141. DOI 10.1007/s00158-016-1574-3.

22. Zhao, J., Yoon, H., Youn B, D. (2020). An adaptive hybrid expansion method (ahem) for efficient structural topology optimization under harmonic excitation. *Structural and Multidisciplinary Optimization, 61(3),* 895–921. DOI 10.1007/s00158-019-02457-7.

23. Liu, H., Zhang, W., Gao, T. (2015). A comparative study of dynamic analysis methods for structural topology optimization under harmonic force excitations. *Structural and Multidisciplinary Optimization, 51(6),* 1321–1333. DOI 10.1007/s00158-014-1218-4.

24. Ma, Z. D., Kikuchi, N., Cheng, H. C. (1995). Topological design for vibrating structures. *Computer Methods in Applied Mechanics Engineering, 121,* 259–280. DOI 10.1016/0045-7825(94)00714-X.

25. Pedersen, N. L. (2000). Maximization of eigenvalues using topology optimization. *Structural and Multidisciplinary Optimization, 20,* 2–11. DOI 10.1007/s001580050130.

26. Niu, B., Yan, J., Cheng, G. D. (2009). Optimum structure with homogeneous optimum cellular material for maximum fundamental frequency. *Structural and Multidisciplinary Optimization, 39,* 115–32. DOI 10.1007/s00158-008-0334-4.

27. Huang, X. D., Zuo, Z. H., Xie, Y. M. (2010). Evolutionary topological optimization of vibrating continuum structures for natural frequencies. *Composite Structures, 88,* 357–364. DOI 10.1016/j.compstruc.2009.11.011.

28. Xia, Q., Shi, T., Wang, M. Y. (2011). A level set based shape and topology optimization method for maximizing the simple or repeated first eigenvalue of structure vibration. *Structural and Multidisciplinary Optimization, 43,* 473–485. DOI 10.1007/s00158-010-0595-6.

29. Li, Z., Shi, T., Xia, L., Xia, Q. (2019). Maximizing the first eigenfrequency of structures subjected to uniform boundary erosion through the level set method. *Engineering with Computers, 35,* 21–33. DOI 10.1007/s00366-018-0580-z.

30. Du, J. B., Olhoff, N. (2007). Topological design of freely vibrating continuum structures for maximum values of simple and multiple eigenfrequencies and frequency gaps. *Structural and Multidisciplinary Optimization, 34,* 91–110. DOI 10.1007/s00158-007-0101-y.

31. Li, Q. H., Wu, Q. B., Liu, J., He, J. J., Liu, S. T. (2021). Topology optimization of vibrating structures with frequency band constraints. *Structural and Multidisciplinary Optimization, 63,* 1203–1218. DOI 10.1007/s00158-020-02753-7.

32. Ye, H. L., Shen, J. X., Sui, Y. K. (2012). Dynamic topological optimal design of three-dimensional continuum structures with frequencies constraints. *Chinese Journal of Theoretical and Applied Mechanics, 44(6),* 1037–1045. DOI 10.6052/0459-1879-12-069.

33. Long, K., Gu, X. G., Wang, X. (2017). Light weight design method for continuum structure under vibration using multiphase materials. *Acta Aeronautica et Astronautica Sinica, 38,* 129–138. DOI 10.7527/S1000-6893.2017.221022.

34. Zargham, S., Ward, T. A., Ramli, R., Badruddin, I. A. (2016). Topology optimization: A review for structural designs under vibration problems. *Structural and Multidisciplinary Optimization, 53,* 1157–1177. DOI 10.1007/s00158-015-1370-5.

35. Ma, Z. D., Kikuchi, N., Hagiwara, I. (1993). Structural topology and shape optimization for a frequency response problem. *Computational Mechanics, 13,* 157–174. DOI 10.1007/BF00370133.

36. Olhoff, N., Du, J. (2014). Introductory notes on topological design optimization of vibrating continuum structures. In: Rozvany, G. I. N., Lewiński, T. (Eds), *Topology optimization in structural and continuum mechanics*, vol. 549, pp. 259–273. Vienna: Springer. DOI 10.1007/978-3-7091-1643-2_10.

37. Long, K., Wang, X., Liu, H. (2019). Stress-constrained topology optimization of continuum structures subjected to harmonic force excitation using sequential quadratic programming. *Structural and Multidisciplinary Optimization, 59(5),* 1747–1759. DOI 10.1007/s00158-018-2159-0.

38. Zhu, J. H., Zhang, W. H., Qiu, K. P. (2005). Investigation of localized modes in topology optimization of dynamic structures. *Acta Aeronautica et Astronautica Sinica, 26,* 619–623. DOI 10.1677/jme.1.02008.

39. Silva, O. M., Neves, M. M., Lenzi, A. (2019). A critical analysis of using the dynamic compliance as objective function in topology optimization of one-material structures considering steady-state forced vibration problems. *Journal of Sound and Vibration, 444,* 1–20. DOI 10.1016/j.jsv.2018.12.030.

40. Liu, J. K., Ma, Y. S. (2016). A survey of manufacturing oriented topology optimization methods. *Advances in Engineering Software, 100,* 161–175. DOI 10.1016/j.advengsoft.2016.07.017.

41. Zhang, W. S., Li, D., Zhang, J. X., Guo, X. (2016). Minimum length scale control in structural topology optimization based on the moving morphable components (MMC) approach. *Computer Methods in Applied Mechanics Engineering, 311,* 327–355. DOI 10.1016/j.cma.2016.08.022.

42. Sigmund, O. (2007). Morphology-based black and white filters for topology optimization. *Structural and Multidisciplinary Optimization, 33,* 401–424. DOI 10.1007/s00158-006-0087-x.

43. Xu, S., Cai, Y., Cheng, G. D. (2010). Volume preserving nonlinear density filter based on heaviside functions. *Structural and Multidisciplinary Optimization, 41,* 495–505. DOI 10.1007/s00158-009-0452-7.

44. Wang, F., Lazarov, B. S., Sigmund, O. (2011). On projection methods, convergence and robust formulations in topology optimization. *Structural and Multidisciplinary Optimization, 43,* 767–784. DOI 10.1007/s00158-010-0602-y.

45. Yang, K., Fernandez, E., Niu, C., Duysinx, P., Zhu, J. H. et al. (2019). Note on spatial gradient operators and gradient-based minimum length constraints in SIMP topology optimization. *Structural and Multidisciplinary Optimization, 60,* 393–400. DOI 10.1007/s00158-019-02269-9.

46. Zhang, W., Zhong, W., Xu, G. (2014). An explicit length scale control approach in SIMP-based topology optimization. *Computer Methods in Applied Mechanics Engineering, 282,* 71–86. DOI 10.1016/j.cma.2014.08.027.

47. Hägg, L., Wadbro, E. (2018). On minimum length scale control in density based topology optimization. *Structural and Multidisciplinary Optimization, 58,* 1015–1032. DOI 10.1007/s00158-018-1944-0.

48. Cheng, G. D., Liu, X. F. (2011). Discussion on symmetry of optimum topology design. *Structural and Multidisciplinary Optimization, 44,* 713–717. DOI 10.1007/s00158-011-0686-z.

49. Guo, X., Ni, C., Cheng, G. D., Du, Z. (2012). Some symmetry results for optimal solutions in structural optimization. *Structural and Multidisciplinary Optimization, 46,* 631–645. DOI 10.1007/s00158-012-0802-8.

50. Stolpe, M. (2010). On some fundamental properties of structural topology optimization problems. *Structural and Multidisciplinary Optimization, 41,* 661–670. DOI 10.1007/s00158-009-0476-z.

51. Liang, Y., Cheng, G. D. (2019). Topology optimization via sequential integer programming and canonical relaxation algorithm. *Computer Methods in Applied Mechanics Engineering, 348,* 64–96. DOI 10.1016/j.cma.2018.10.050.

52. Liang, Y., Cheng, G. D. (2020). Further elaborations on topology optimization via sequential integer programming and canonical relaxation algorithm and 128-line MATLAB code. *Structural and Multidisciplinary Optimization, 61,* 411–431. DOI 10.1007/s00158-019-02396-3.

53. Liang, Y., Sun, K., Cheng, G. D. (2020). Discrete variable topology optimization for compliant mechanism design via sequential approximate integer programming with trust region (SAIP-TR). *Structural and Multidisciplinary Optimization, 62,* 2851–2879. DOI 10.1007/s00158-020-02693-2.

54. Svanberg, K., Werme, M. (2007). Sequential integer programming methods for stress constrained topology optimization. *Structural and Multidisciplinary Optimization, 34,* 277–299. DOI 10.1007/s00158-007-0118-2.

55. Jog, C. S. (2009). A dual algorithm for the topology optimization of non-linear elastic structures. *International Journal for Numerical Methods in Engineering, 77(4),* 502–517. DOI 10.1002/nme.2422.

56. Huang, X. D., Xie, Y. M. (2007). Convergent and mesh-independent solutions for the bi-directional evolutionary structural optimization method. *Finite Elements in Analysis and Design, 43(14),* 1039–1049. DOI 10.1016/j.finel.2007.06.006.

57. Wang, M. Y., Wang, S. (2010). Bilateral filtering for structural topology optimization. *International Journal for Numerical Methods in Engineering, 63(13),* 1911–1938. DOI 10.1002/nme.1347.

58. Crispo, L., Bohrer, R., Roper, S. W., Kim, I. Y. (2021). Spatial gradient interface detection in topology optimization for an unstructured mesh. *Structural and Multidisciplinary Optimization, 63,* 515–522. DOI 10.1007/s00158-020-02688-z.